Variability, timescales, and non-linearity in climate responses to black carbon emissions

Yang Yang[1*], Steven J. Smith[2*], Hailong Wang[1], Catrin M. Mills[1], Philip J. Rasch[1]

[1]Atmospheric Sciences and Global Change Division, Pacific Northwest National Laboratory, Richland, Washington, USA

[2]Joint Global Change Research Institute, Pacific Northwest National Laboratory, College Park, Maryland, USA

*Correspondence to yang.yang@pnnl.gov and ssmith@pnnl.gov

Abstract

Black carbon (BC) particles exert a potentially large warming influence on the Earth system. Reductions in BC emissions have attracted attention as a possible means to moderate near-term temperature changes. For the first time, we evaluate regional climate responses, non-linearity, and short-term transient responses to BC emission perturbations in the Arctic, mid-latitudes, and globally based on a comprehensive set of emission-driven experiments using the Community Earth System Model (CESM). Surface temperature responses to BC emissions are complex, with surface warming over land from mid-latitude BC perturbations partially offset by ocean cooling. Climate responses do not scale linearly with emissions. While stronger BC emission perturbations have a higher burden efficiency, their temperature sensitivity is lower. BC impacts temperature much faster than greenhouse gas forcing, with transient temperature responses in the Arctic and mid-latitudes approaching a quasi-equilibrium state with a timescale of 2–3 years. We find large variability in BC-induced climate changes due to background model noise. As a result, removing present-day BC emissions results in discernible surface temperature changes for only limited regions of the globe. In order to better understand the climatic impacts of BC emissions, both the drivers of non-linear responses and response variability need to be assessed across climate models.

1. Introduction

Black carbon (BC) aerosol, emitted from incomplete combustion, may be the second strongest positive anthropogenic climate forcing following carbon dioxide, which drew attention for potential climate mitigation from reducing BC emissions (Jacobson, 2004; Shindell et al., 2012; Bond et al., 2013; Smith and Mizrahi, 2013). The relationship between forcing and surface temperature changes caused by BC is complex and forcing is not a reliable indicator of the climatic impact of BC emissions (Stjern et al., 2017). BC absorbs solar radiation within the atmospheric column thereby warming the atmosphere with an influence on surface temperature that depends on its vertical location. At high altitudes, BC cools the surface by absorbing solar radiation (i.e., blocking it from reaching the surface) (Ramanathan and Carmichael, 2008), while BC at low altitudes warms the surface through diabatic heating (Ban-Weiss et al., 2012). In addition, heating the atmosphere and cooling the surface can increase atmospheric stability and therefore affect cloud formation, lifetime, and dynamical processes (Koren et al., 2004; McFarquhar and Wang, 2006; Koch and Del Genio, 2010). Through transformation from hydrophobic aggregates to hydrophilic particles coated with water-soluble substances (*i.e.,* aging processes), BC can become cloud-nucleating particles (Oshima et al., 2009), alter cloud microphysical processes, and suppress precipitation (Boucher et al., 2013). BC-induced warming or cooling can increase or decrease surface evaporation, resulting in further changes in precipitation and cloud formation (McFarquhar and Wang, 2006; Andrews et al., 2010; Ming et al., 2010; Ban-Weiss et al., 2012;

61 Kvalevåg et al., 2013). BC can also decrease surface albedo through deposition on

62 snow and ice, which is especially important to the climate at high latitudes and,

63 particularly the Arctic (Flanner et al., 2007; Qian et al., 2014) as snow/ice-albedo

64 effects are strong there. Taken together, these processes result in interactions

65 between BC and the atmosphere that can ultimately alter the net impact of BC on

66 climate, which have been termed rapid adjustments (Stjern et al., 2017).

67   Studies found that increases in BC emissions may contribute to the amplification

68 of Arctic warming directly by absorbing solar radiation in the atmosphere and

69 indirectly by reducing surface albedo through deposition on snow and ice (Flanner et

70 al., 2007; Qian et al., 2014). Flanner (2013) highlighted the importance of BC vertical

71 location in Arctic climate responses, with surface warming (cooling) due to BC in the

72 lower (upper) troposphere. In addition, BC outside the Arctic can influence the Arctic

73 climate through changing poleward heat transport. With BC snow/ice-albedo effect

74 excluded, Shindell and Faluvegi (2009) modeled an Arctic surface warming (cooling)

75 due to reducing (enhancing) mid-latitude BC atmospheric concentrations. Sand et al.

76 (2013a) found that this was due to the increased northward heat transport into the

77 Arctic. However, in another study where BC emissions were perturbed instead of

78 concentrations, Sand et al. (2013b) reported a decrease in northward heat transport

79 due to increases in mid-latitude BC emissions and suggested that the heating effect

80 of BC transported to the Arctic dominated the Arctic heating in the mid-latitude

81 perturbation simulation, leading to the opposite direction of atmospheric heat

82 transport compared to the concentration-driven perturbations. They also found that

83   increases in both BC emission and BC concentration in the Arctic atmosphere may

84   weaken poleward heat transport due to increasing Arctic temperature driven by BC

85   heating in the atmosphere and on snow and ice surfaces. Therefore, understanding

86   the Arctic climate impact of regional BC emissions is important for the Arctic climate

87   mitigation (Sand et al., 2016).

88   In order to archive a statistically significant signal for Arctic surface temperature

89   responses to BC emissions, Sand et al. (2013b) scaled present-day BC emissions

90   within the Arctic by a factor of 150 and emissions from mid-latitudes by a factor of 9,

91   respectively, in the NorESM model with BC snow/ice-albedo effects included. They

92   found that emissions of BC within the Arctic have an Arctic surface temperature

93   response 5 times larger than those from mid-latitudes and attributed this to BC

94   snow/ice-albedo feedbacks. The impact of BC emission perturbations on

95   mid-latitudes were not examined in that study, which we do in this work to contrast

96   the impact of BC on the Arctic with mid-latitudes.

97   Much of the previous work on BC has used atmosphere-only models or

98   prescribed BC concentrations (Hansen et al., 2005; Ming et al., 2010; Ban-Weiss et

99   al., 2012; Sand et al., 2013a), which artificially reduces variability in model results.

100   Results qualitatively differ between prescribed BC-concentration and emission-driven

101   simulations with coupled models (Sand et al., 2013a,b, 2015). A previous study using

102   coupled models found that the BC response in three of these models showed high

103   variability and inconsistency in the net sign of the responses to present-day BC

104   emissions both between models and even between ensemble members from the

105   same model (Baker et al., 2015). Stjern et al. (2017) investigated climate responses

106   to a tenfold increase in present-day anthropogenic BC concentrations or emissions

107   using five concentration-driven and four emission-driven global climate models. They

108   found that low-level cloud amounts increase, while higher-level clouds are diminished

109   for all models, which is dominated by rapid adjustments. The negative rapid

110   adjustments from changing clouds dampened positive instantaneous radiative forcing

111   of BC at the TOA, leading to a relatively small global surface warming. However, this

112   study did not consider response variability or non-linearity of responses. We note that

113   the model used in our study contains a different aerosol treatment (see below) than

114   the model used in Stjern et al. (2015).

115   To better understand the impacts of BC on climate, we present a comprehensive

116   analysis using a set of coupled simulations that examine regional climate responses,

117   non-linearity, and short-term transient climate responses to BC emission

118   perturbations. We focus in particular on the Arctic and also variability to assess if

119   climate responses to BC emission changes are likely to be discernable. Only

120   combustion and process-based anthropogenic BC emissions are perturbed, given

121   that the net global climate impact of open burning emissions has been assessed to be

122   small due to their high organic carbon fraction. A summary of key results is provided

123   below.

124

125   **2. Methods**

126   **2.1 Model description**

127   Here we use the fully coupled CESM (Community Earth System Model; Hurrell et

128   al., 2013) to simulate climate responses to BC emission perturbations. In

129   CAM5-MAM4 (Community Atmosphere Model version 5), the atmospheric

130   component of CESM, mass and number concentrations of aerosols are predicted

131   within four lognormal modes (i.e., Aitken, accumulation, coarse, and primary carbon

132   mode) of the modal aerosol module (MAM4; Liu et al., 2016). BC is emitted into the

133   primary-carbon mode and aged into the accumulation mode when coated with sulfate

134   or secondary organic aerosol. Particles in the accumulation mode, including BC and

135   other species, can serve as cloud condensation nuclei and have microphysical

136   effects on stratiform clouds and precipitation. The model physically treats

137   aerosol-cloud interactions using two-moment stratiform cloud microphysics, which

138   predicts number concentrations and mixing ratios of cloud water and ice (Morrison

139   and Gettelman, 2008; Gettelman et al., 2010). Activation of stratiform cloud droplets

140   is based on the scheme of Abdul-Razzak and Ghan (2000). In addition to the

141   standard treatments of aerosol-cloud interactions, we also include a set of

142   modifications that improves the simulation of aerosol wet scavenging and convective

143   transport (Wang et al., 2013). Although aerosols have no microphysical impact on

144   convective clouds, BC induced atmospheric heating can affect the ambient

145   temperature and convection. Convective precipitation can scavenge and remove

146   aerosols. Previous studies have extensively evaluated the CAM5 model simulations

147   of concentration, deposition, vertical profile and optical properties of BC (Wang et al.,

148   2013; Wang et al., 2015; Zhang et al., 2015a,b; Liu et al., 2016; Yang et al., 2017,

149   2018a,b)), as well as climate variables (Hurrell et al., 2013; Yang et al., 2016a,b).

150   The model can simulate well the BC aerosol and climate variables in most regions of

151   the globe, but was reported to underestimate BC concentrations over China (Yang et

152   al., 2018a) and the Arctic (Wang et al., 2013) (although this earlier study used a

153   different emissions dataset), implying a possible underestimate of climate responses

154   to BC emissions in this study.

155   In our model simulations, atmospheric radiative transfer is calculated twice with

156   BC included and excluded, respectively. The changes in direct radiative effect and

157   cloud radiative effect induced by BC perturbation are calculated as $\Delta(F_{clear} - F_{clear,clean})$

158   and $\Delta(F_{clean} - F_{clear,clean})$, respectively, where F_{clear} is the TOA flux calculated

159   neglecting scattering and absorption by clouds, F_{clean} is the TOA flux calculated

160   neglecting scattering and absorption by BC, $F_{clear,clean}$ is the TOA flux calculated

161   neglecting scattering and absorption by both clouds and BC, and Δ refers to the

162   differences between the control and one of the emission perturbed simulations (Ghan,

163   2013). Note that these quantities include the impact of slow responses and feedbacks

164   (e.g., changes in sea surface temperature and sea ice and feedbacks with clouds) so

165   are not strictly comparable to the conventional definition of radiative forcing (Boucher

166   et al., 2013). The BC snow/ice-albedo effect on top of land and sea ice is included in

167   the model (Flanner et al., 2007; Yang et al., 2017, 2018c).

168   **2.2 Experimental configuration and emissions**

169   The following simulations are performed in this study. All insolation, greenhouse

170   gas concentrations and aerosol and precursor emissions, except BC, are fixed at

171   year 1850 levels, which include open burning emissions (van Marle et al., 2017).

172   The MID7X and ARC150X simulations use large emission perturbations to result

173   in signals large enough for detailed analysis. These regions are also particularly

174   important for BC impacts on the Arctic. The multipliers were selected following Sand

175   et al. (2013b) with the expectation that these would result in similar radiative

176   perturbations. This also allows a direct comparison to these previous results (Sand et

177   al., 2013b; and also Baker et al., 2015), which are also BC-emission simulations

178   using a coupled model with snow/ice-albedo feedbacks. The PD simulation then

179   allows us to evaluate the impact of present-day anthropogenic emissions. In brief, the

180   simulations conducted are:

181   1. PD: control simulation for BC in present-day conditions. BC emissions are

182   fixed at year 2010 (average of 2008–2012).

183   2. ARC150X: perturbed simulation to quantify the climate responses to Arctic BC

184   emissions. Same as PD except that year 2010 level anthropogenic BC

185   emissions over the Arctic (60–90°N) are scaled by a factor of 150.

186   3. MID7X: perturbed simulation to quantify the climate responses to mid-latitude

187   BC emissions. Same as PD except that year 2010 level anthropogenic BC

188   emissions over the mid-latitudes (28–60°N) are scaled by a factor of 7.

4. ARC75X: perturbed simulation to quantify non-linearity of climate responses to Arctic BC emissions. Same as ARC150X except that Arctic BC emissions are scaled by a factor of 75.

5. MID3.5X: perturbed simulation to quantify non-linearity of climate responses to mid-latitude BC emissions. Same as MID7X except that mid-latitude BC emissions are scaled by a factor of 3.5.

6. MID14X: perturbed simulation to quantify non-linearity of climate responses to mid-latitudes BC emissions. Same as MID7X except that mid-latitude BC emissions are scaled by a factor of 14.

7. PI: sensitivity simulation for BC in preindustrial conditions to compare results with Baker et al. (2015). BC emissions are at year 1850 levels.

Both mass and number of BC emissions are perturbed proportionally. Each simulation has one ensemble member for 100 years which are branched from year 81 of the PI simulation after 80 years spin-up, with the last 80 years used for most analysis. Another four short-term ensemble members for 30 years are conducted under both ARC150X and MID7X to examine the short-term transient climate response to BC emissions. These are branched from years 96, 112, 120, and 140 of PI simulation.

The CEDS (Community Emissions Data System) anthropogenic emissions (Hoesly et al., 2018) (version 2017-05-18) that were developed for the CMIP6 (Coupled Model Intercomparison Project Phase 6) model experiments are used in our simulations. Note that this emission dataset includes monthly BC emission

211 seasonality, which has been shown to be important for simulating BC in the Arctic

212 (Stohl et al., 2013). Figure S1 shows spatial distribution of annual anthropogenic BC

213 emissions for year 2010 (average of 2008–2012) and the regions for BC emission

214 perturbation. Over 60–90°N, anthropogenic BC emissions are mostly over the lower

215 latitude of the Arctic (60–70°N). Over the mid-latitudes, high BC emissions are mainly

216 located over eastern China. The annual total anthropogenic BC emission from the

217 Arctic in year 2010 is 0.08 Tg C yr^{-1}, with 70% contributed by energy sector. Scaled

218 by a factor of 150, ARC150X has 12.63 Tg C yr^{-1} more BC emissions than the PD in

219 the Arctic. About 3.46 Tg C yr^{-1} of BC is emitted from the mid-latitudes, with the

220 largest contribution from the residential sector (36%). With a scaling factor of 7,

221 MID7X includes an additional 20.74 Tg C yr^{-1} of BC emission from mid-latitudes, as

222 compared to PD. Global annual anthropogenic BC for PD is 7.72 Tg C yr^{-1}, much

223 higher than 0.92 Tg C yr^{-1} for PI.

224

225 **3. Regional climate responses to increases in Arctic and mid-latitude BC**

226 **emissions**

227   We first examine results from simulations with large perturbations of Arctic and

228 mid-latitude BC emissions (ARC150X and MID7X). Our initial simulations focused on

229 these regions due to the potentially high sensitivity of the Arctic to BC emissions.

230 Figure 1 presents the increases in annual, zonal-mean BC concentrations from

231 ARC150X and MID7X simulations, as compared to PD. Both Arctic and mid-latitude

232 BC emissions lead to BC concentration increases in the entire Northern Hemisphere,

233   with Arctic emissions mainly impacting low altitudes within the Arctic. In ARC150X,

234   due to extremely low temperatures at the surface and therefore temperature

235   inversions and a transport barrier (so called Arctic front), BC concentration increases

236   are mainly located over low altitudes within the Arctic. In MID7X, increased

237   mid-latitude emissions produce large increases in BC concentrations between 30°–

238   45°N. BC emitted over the mid-latitudes, which is lifted above the boundary layer and

239   transported at higher altitudes into the Arctic, leading to increased concentrations of

240   BC in the Arctic atmosphere. This spatial pattern is similar to that in Sand et al.

241   (2013b).

242   To explore the importance of emissions from these source regions to BC column

243   burdens, Table 1 summarizes BC burden efficiency, which is defined as the changes

244   in regional mean column burden of BC produced by per unit emission change,

245   calculated by differences between the perturbed and PD simulation. Over the Arctic,

246   increases in Arctic local BC emissions lead to an Arctic column burden efficiency of

247   0.425 ±0.024 mg m^{-2} (Tg yr^{-1})$^{-1}$. The burden efficiency of mid-latitude emissions over

248   the mid-latitudes is 0.191 ±0.004 mg m^{-2} (Tg yr^{-1})$^{-1}$, less than half of the efficiency of

249   Arctic emission on Arctic burden due to lower precipitation and frequent temperature

250   inversion in the Arctic compared to mid-latitudes. While the relative impact of

251   mid-latitude emissions on the Arctic burden efficiency (0.106 ±0.004 mg m^{-2} (Tg yr^{-1})$^{-1}$)

252   is smaller than either of the above efficiencies, the 28 times larger present-day total

253   emissions from mid-latitudes (3.70 Tg yr^{-1}) than the Arctic (0.13 Tg yr^{-1}) dominate

254   column burden contributions.

255   Table 1 also summarizes the changes in BC direct radiative effect, cloud radiative

256   effect, and snow/ice-albedo forcing induced by these large BC perturbations. Note

257   that these values include feedback effects from the coupled system, so are not

258   comparable to conventionally defined radiative forcing values. The albedo change

259   due to BC deposition on snow and ice is responsible for a significant increase in

260   Arctic surface forcing in both perturbations, with far smaller changes per unit emission

261   in mid-latitudes. Positive changes in direct radiative effect are offset by negative

262   changes in cloud radiative effect from increases in low cloud in the Arctic and

263   decreases in mid-level and high cloud over the mid-latitudes, similar to previous

264   results with a tenfold increase in present-day anthropogenic BC emissions (Stjern et

265   al., 2017).

266   Forcing efficiencies for direct radiative effect, cloud radiative effect and

267   snow/ice-albedo forcing (i.e., forcings produced by per unit emission change) are also

268   summarized in Table 1. Over the Arctic, local emissions from the Arctic have 2–4

269   times higher forcing efficiencies than emissions from the mid-latitudes, suggesting

270   higher impacts of a unit Arctic BC emission change to Arctic energy balance. Over the

271   mid-latitudes, although forcing efficiencies for direct radiative and cloud radiative

272   effects for Arctic emissions are 2–3 times lower than mid-latitude emissions, the

273   snow/ice-albedo forcing efficiencies are similar between Arctic and mid-latitude

274   emissions.

275   The annual mean surface air temperature response in ARC150X shows a

276   significant warming over both the Arctic and mid-latitudes (Figure 2). MID7X shows

13

277   temperature increases over the Arctic and most of the mid-latitude land regions, while

278   surface temperature decreases over some oceanic and coastal areas. The presence

279   of areas with both surface warming and cooling decreases the net average

280   temperature change over mid-latitudes. The seasonal mean surface air temperature

281   responses present similar spatial patterns (Figure S2), but slightly different

282   magnitudes (Figure S3). Over the Arctic, the warming due to Arctic BC emissions is

283   weakest in boreal summer. This is because the smaller summer sea ice and snow

284   fraction in the Arctic weakens BC snow/ice-albedo forcing. However, in the

285   mid-latitudes, warming is strongest in boreal summer for both Arctic and mid-latitude

286   BC emissions, because of stronger summer solar insolation and, therefore, stronger

287   BC heating in the atmosphere.

288   Due to the increased atmospheric absorption from BC, northward heat transport

289   for both perturbations decreases (Figure 3), consistent in sign with the results of Sand

290   et al. (2013b). The increases in temperature but decreases in net northward heat

291   transport indicate that the heating induced by changes in BC direct radiative effect

292   and BC snow/ice-albedo forcing dominate the overall BC-induced changes in energy

293   balance over the Arctic and mid-latitudes.

294   Arctic emissions are more efficient at impacting Arctic surface air temperatures

295   with an Arctic temperature sensitivity to Arctic emissions (0.169 ± 0.052 K (Tg yr^{-1})$^{-1}$)

296   seven times as large as the Arctic temperature sensitivity to mid-latitude emissions

297   (0.023 ± 0.038 K (Tg yr^{-1})$^{-1}$). Mid-latitude emissions, however, are likely to have a

298   larger present-day impact overall due to their 35 times larger preindustrial to

299   present-day emission increase (2.874 Tg yr^{-1}) than Arctic emissions (0.082 Tg yr^{-1}).

300   Note that, the Arctic temperature sensitivities are about 30% and 50% smaller than

301   those found in the coupled NorESM model experiments of Sand et al. (2013b) for

302   Arctic and mid-latitude emission perturbation simulations, respectively, probably due

303   to different model parameterizations and/or different vertical profile of BC driving the

304   net effect of BC impact on Arctic surface temperature (Flanner, 2013).

305   The vertical distribution of annual, zonal mean temperature responses (Figure 4)

306   shows that the ARC150X leads to a strong warming from the surface to 400 hPa over

307   the Arctic and between 40°–60°N. In MID7X, although the zonal mean surface

308   temperature response is relatively weak compared to ARC150X, a significant

309   warming is found in mid-latitudes between 500 and 200 hPa. BC transported from

310   mid-latitudes into the Arctic at high altitudes also results in Arctic temperature

311   increases aloft, between 400 and 300 hPa.

312   These changes in temperature pattern can change the stability of the atmosphere

313   and impact atmospheric circulation, as shown in Figure 5. Increases in BC emissions

314   over both the Arctic and mid-latitudes exert anomalous upward motions in the Arctic

315   and downward motions over the mid-latitudes, but for different reasons. In ARC150X,

316   stronger warming at the Arctic surface, compared to high altitudes, likely due to the

317   BC snow/ice-albedo effect, produces anomalous upward motions in the Arctic and

318   compensating downward motions between 50°–60°N. In MID7X, the stronger BC

319   warming at higher altitudes in mid-latitudes increases atmospheric stability and leads

320   to strong anomalous downward motions between 40°–60°N and compensating

321 upward motions over the Arctic and 10°–30°N (Johnson et al., 2004). Increasing

322 surface temperature and anomalous upward motion over the Arctic can weaken the

323 Arctic front, and the anomalous downward motion over the mid-latitudes favors air

324 stagnation.

325   Because of the anomalous downward motions over mid-latitudes in both

326 ARC150X and MID7X, high and/or mid-level cloud fraction decrease over

327 mid-latitudes (Figure 6). Due to slow feedbacks from increases in surface

328 temperature in the Arctic (Figure 2) and decreases in snow and sea ice, low cloud

329 fraction increases in the Arctic for both ARC150X and MID7X. The increases in low

330 cloud over mid-latitude oceans, which cause the cooling noted above, are due to

331 rapid adjustments as free-tropospheric BC heating reduces mixing with dry air above

332 the BC layer and increases the amount of marine stratocumulus (Johnson et al., 2004;

333 Sand et al., 2013a; Stjern et al., 2017).

334   Figure 7 shows changes in the total precipitation rate for the perturbed

335 simulations. Increases in Arctic and mid-latitude BC emissions lead to significant

336 decreases in precipitation over 60°N and 30–50°N, respectively, in correspondence

337 with anomalous downward motions (Figure 5) and decreases in mid-level and high

338 clouds (Figure 6) over these regions. Averaged over the Arctic and mid-latitudes,

339 changes in precipitation are weak, compared to uncertainties, except for the

340 mid-latitude precipitation response to BC emitted from mid-latitudes. The mid-latitude

341 precipitation sensitivity is -7.67 (± 3.34) µm day^{-1} (Tg yr^{-1})$^{-1}$ for MID7X. Another

342 feature of the precipitation response is related to a northward shift in the ITCZ

343   (Intertropical Convergence Zone) in MID7X, which is consistent with the

344   hemispherically asymmetric warming pattern driven by increases in mid-latitude BC

345   emissions (Hwang et al., 2013; Baker et al., 2015).

346   Both ARC150X and MID7X show significant decreases by 13% and 3%,

347   respectively, in fractional area covered by sea ice over the Arctic, as compared to PD

348   (Figure S4). The snow depth over land also decreases, especially over Greenland.

349   The water equivalent snow depth averaged over Arctic land decreases by 5.0 cm (27%

350   relative to PD) and 0.8 cm (4%), respectively, for ARC150X and MID7X.

351

352   **4. Non-linearity of climate responses.**

353   We also evaluated the linearity of these responses by testing different emission

354   perturbation sizes. Figure 8 shows burden efficiencies, temperature and precipitation

355   sensitivities from simulations with Arctic BC emissions scaled by 75 and 150,

356   respectively, and mid-latitude BC emissions scaled by 3.5, 7 and 14, respectively,

357   with values summarized in Table 2. Stronger emission perturbations have a higher

358   burden efficiency. Over the Arctic, this is caused by anomalous Arctic upward

359   motions that weaken the Arctic front, lifting BC higher and leading to a longer BC

360   lifetime together with easier transport into the Arctic (Figure S5). Over mid-latitudes,

361   anomalous mid-latitude downward motions favor stagnation, which in turn

362   accumulates more BC in the atmosphere, together with decrease in precipitation (and

363   wet removal rate), contributing to increases in burden efficiency. All differences in

364 burden efficiencies between simulations with different emission perturbation sizes are

365 statistically significant with 95% confidence.

366   Despite this higher burden efficiency, the efficiency (per unit emission) of the

367 direct radiative effect decreases slightly. This is because strong BC perturbations

368 lead to more BC suspended in the atmosphere. More BC increases the attenuation of

369 the transmitted radiation, leading to a decrease in efficiency of BC light absorption in

370 the lower atmosphere and leading to a lower efficiency of direct radiative effect for a

371 stronger BC emissions perturbation.

372   The temperature sensitivity is lower, with 95% significance, for stronger

373 emission perturbations for both mid-latitude and Arctic BC between ARC75X and

374 ARC150X, as well between MID7X and MID14X (Table 2). The BC snow/ice-albedo

375 effect is found to be the most important factor in influencing Arctic temperature (Sand

376 et al., 2013b). Larger temperature increases from stronger BC emission perturbations

377 speed up sea ice and snow melt, leading to a weaker annual mean snow/ice-albedo

378 effect per unit BC emission for both Arctic and mid-latitudes. Therefore, the BC

379 snow/ice-albedo effect is more efficient for weaker emission perturbations, i.e., 0.151

380 ($\pm$0.011) vs. 0.099 ($\pm$0.006) (W m^{-2} (Tg yr^{-1})$^{-1}$) for ARC75X and ARC150X and 0.026

381 ($\pm$0.002) vs. 0.020 ($\pm$0.002) (W m^{-2} (Tg yr^{-1})$^{-1}$) for MID7X and MID14X of Arctic BC

382 snow/ice-albedo forcing efficiencies. All snow/ice-albedo forcing efficiency

383 differences are statistically significant. Together with lower efficiency of the direct

384 radiative effect, these explain the lower temperature sensitivity for stronger emission

385 perturbation. The non-linearity in snow-ice feedback relative to emissions size

386 appears to be the primary driver of surface temperature response non-linearity in

387 these results.

388   Additional evidence for BC non-linearity can be found in the literature. Sand et al.

389 (2015) simulated climate responses to BC in NorESM with present-day emissions

390 multiplied by 25 and reported that the changes in TOA net shortwave flux was 7.5

391 (±0.3) W m^{-2} relative to preindustrial conditions and the temperature response was

392 1.2 (±0.1) K. If we assume a linear emission-response relationship, present-day BC

393 would cause an inferred shortwave flux and surface temperature change of 0.312

394 (±0.013) W m^{-2} and 0.050 (±0.004) K in Sand et al. (2015), much lower than the 0.552

395 W m^{-2} and 0.141 K found in Baker et al. (2015) for a present-day BC emission

396 perturbation with essentially the same model. Note that the change in shortwave flux

397 is not proportional to the surface temperate change, further emphasizing that forcing

398 is not a good predictor of surface temperature change for BC. This comparison is

399 consistent with our finding that temperature sensitivity is lower for stronger BC

400 emission perturbations. We note, however, that emission datasets with different

401 spatial distributions and seasonality were used in those two experiments (because of

402 this the difference in global emissions between the two experiments is about 17, not

403 25 times). While this might impact the magnitude of model responses, it is unlikely to

404 change the overall conclusion of a substantially different temperature response to

405 current-day emissions as compared to a 17–25 times larger BC perturbation.

406   The mid-latitude shows significantly stronger precipitation sensitivity for a

407 stronger perturbation, comparing MID7X and MID14X, which is consistent with the

408 higher burden efficiency. This is in the opposite direction to the surface temperature

409 sensitivity. Variability in MID3.5X is larger than the mean value for both temperature

410 and precipitation sensitivity, which highlights the challenge of testing differences for

411 smaller BC perturbation magnitudes. Note that the impact of BC on clouds and

412 precipitation is uncertain, especially in the Arctic, due to the limited treatment of Arctic

413 clouds in climate models (McFarquhar et al., 2011). These results suggest that in

414 order to examine the climate responses to BC emissions in short-term climate model

415 simulations, a large emission perturbation is needed to get a clear signal, but

416 non-linearity of the responses also needs to be evaluated.

417

418 **5. Short-term transient climate responses**

419   To assess the short-term transient climate responses to BC emissions, Figure 9

420 shows surface temperature responses to BC emissions from ARC150X and MID7X

421 for the first 30 years averaged over five short ensemble members. We also show a

422 numerical fit to the short-term transient response using a Hamiltonian Monte Carlo

423 technique (Betancourt, 2017). We fit to the following form:

424                              $T_{ave} (1 - e^{-t/\tau})$,

425 where we have constrained the fit to converge to the long-term average temperature

426 response (T_{ave}) by our finding that there is no detectable long-term trend after the

427 initial transient period over a 100-year time horizon.

428   Over both the Arctic and mid-latitudes, transient temperature responses quickly

429 approach a quasi-equilibrium state. Transient timescales (τ) for the ARC150X

430   perturbation were estimated to be 2.7 (2.0, 3.4) years, while the mid-latitude

431   timescales for the ARC150X and MID7X perturbations were 1.8 (1.1, 2.2) and 2.9

432   (1.2, 4.2) years respectively (brackets provide 10-90% fitting intervals). The Arctic

433   response to MID7X was too noisy to produce a fit. These timescales are shorter than

434   those in a global BC perturbation experiment (Sand et al., 2015), which is expected

435   as ocean thermal inertia would play a larger role globally as compared to the Northern

436   Hemisphere or Arctic. The BC response timescales here are also shorter than those

437   seen from CO_2 concentration steps in GCMs (Geoffroy et al., 2013). There is also no

438   long-term temperature increase, at least over a 100-year time horizon, after the initial

439   transient period. A linear fit over years 10-100 for the perturbation responses results

440   in no statistically significant linear trends for any of the four perturbations (see SI

441   code).

442   Note that the average of even five ensemble members shows oscillatory behavior

443   due to the imposition of a step BC emission perturbation. This oscillatory behavior

444   degrades our ability to quantify the perturbation response timescale. In future work, a

445   linearly phased-in perturbation might result in a cleaner signal for determining the

446   initial response time-scale.

447

448   **6. Climate responses to present-day anthropogenic BC emissions**

449   Baker et al. (2015) showed that the climate responses to BC emissions had very

450   large uncertainties based on results from four global models. Here, we also quantified

451   the impact of present-day anthropogenic BC emissions (Figure 10) by comparing a

452 present-day (PD) and pre-industrial (PI) simulation conducted with the

453 CESM-CAM5-MAM4 model used in this work. PD emissions produce statistically

454 significant surface air temperature changes over only limited regions in the Northern

455 Hemisphere. Decreased temperatures are found over eastern China, South Asia,

456 North Atlantic Ocean, and North American Arctic, partly due to cloud changes driven

457 by BC rapid adjustments. Increased temperatures are found over the Tibetan Plateau,

458 Greenland and high-latitude land regions likely because of the BC snow/ice-albedo

459 effect (Figure S6).

460   The spatial pattern is similar to that from the ECHAM6-HAM2 in Baker et al.

461 (2015). Although CESM-CAM5-MAM4 also includes the BC snow/ice-albedo effect,

462 we do not see the strong warming produced in NorESM under present-day BC

463 emissions. In Baker et al. (2015), NorESM had a global net TOA shortwave forcing

464 efficiency of 0.076 W m^{-2} (Tg yr^{-1})$^{-1}$, nominally higher than 0.043 ±0.073 W m^{-2} (Tg

465 yr^{-1})$^{-1}$ calculated in this study with CESM-CAM5-MAM4, although the difference is

466 well within one standard deviation. Longer model runs would be needed to determine

467 if the BC snow/ice-albedo effect is significantly different in CESM and NorESM. In

468 addition, there may be a small contribution from a shorter BC lifetime (7.22 days in

469 CESM-CAM5-MAM4 Vs. 7.82 days in NorESM) that might also help explain the

470 weaker warming in CESM-CAM5-MAM4 as compared to NorESM.

471   We find that variability is substantial in our experiments. Although statistically

472 significant surface temperature changes are found regionally, as mentioned above,

473 large-scale global surface temperature change from current-day BC emissions is

474   statistically indistinguishable from zero (0.006 ±0.238 K globally and 0.020 ±0.346 K

475   for land only). The global temperature response is within the range of –0.085 to 0.152

476   K from the four models in Baker et al. (2015). Even in the large MID7X perturbation,

477   variability is still fairly large relative to the signal (0.45 ±0.27 K for mid-latitude

478   temperate change) and would overwhelm any large-scale signal for more realistic

479   perturbation sizes. Similarly, while the mid-latitude precipitation response to

480   mid-latitude BC emissions is strong for a MID7X perturbation, this would be difficult to

481   detect for a present-day perturbation.

482

7. Conclusions and discussions

484   BC has been estimated to potentially have one of the largest positive (warming)

485   anthropogenic forcing influences. As a result, there has been substantial scientific

486   and policy attention focused on the potential for BC to moderate climate change in the

487   near-term. In this study, for the first time, we conduct a comprehensive set of

488   emission-driven experiments using a leading coupled climate model (CESM). With a

489   comprehensive set of experiments, we examined regional climate responses,

490   non-linearity, and short-term transient responses to BC emission perturbations in the

491   Arctic, mid-latitudes, and globally.

492   With increases in mid-latitude BC emissions, surface air temperature increases

493   over land, while it decreases over oceanic and coastal areas. Increases in Arctic BC

494   emissions lead to warming over both the Arctic and mid-latitudes. Increases in Arctic

495   and mid-latitude BC emissions also decrease precipitation over 60°N and 30–50°N,

496   respectively. Arctic emissions are more efficient in influencing Arctic surface air

497   temperatures compared to mid-latitude emissions, with an Arctic temperature

498   sensitivity to Arctic emissions seven times as large as that to mid-latitude emissions.

499   We find that climate responses do not scale linearity with emissions. While

500   stronger BC emission perturbations have a higher burden efficiency, efficiencies of

501   snow/ice-albedo forcing and direct radiative effect are lower, leading to a lower

502   temperature sensitivity for stronger BC emission perturbations.

503   BC also impacts temperature much faster than greenhouse gas forcing, with

504   transient temperature responses in the Arctic and mid-latitudes approaching a

505   quasi-equilibrium state with a timescale of 2–3 years. While it has previously been

506   found that, globally, aerosols have a faster impact on temperature as compared to

507   greenhouse gases (Shindell., 2014), termed a "geometric effect" (Meinshausen et al.,

508   2011), we find here that BC perturbations have a very short response time,

509   particularly for Arctic and mid-latitude perturbations. This means that previous studies

510   which have implicitly assumed that the temperature response timescales of BC and

511   GHGs are the same (Boucher and Reddy 2008, Stohl et al., 2015) have likely

512   underestimated the short-term impact of BC emission changes.

513   We find large variability in BC-induced climate changes. Baker et al. (2015)

514   provided error bars of global temperature response for different models in their Figure

515   4a. We note, however, that the error bars in Baker et al. are underestimated because

516   of their assumption of independence of all annual data points (note their use of

517    $1\sigma/\sqrt{N}$ in their error bars for Figure 4). Climate model surface temperatures are

518   strongly correlated over short time scales, which means that instead of the number of

519   data points, a more appropriate measure is the effective number of independent data

520   points (N_{eff}). The 100-year model runs examined here do not provide enough data for

521   this calculation. (Note that we were able to estimate N_{eff} for the 300-year CESM

522   control run from CMIP5, which indicates that runs around 3 times as long as those

523   presented here may be necessary). We, therefore, present standard deviation as a

524   metric of variance.

525   The standard deviation (SD) of global mean surface temperature in PI, PD, and in

526   all of our perturbed simulations is around 0.17–0.19 K, indicating that the dominant

527   source of temperature variability is probably due to internal climate variability or

528   model noise. The SD for temperature responses in perturbed simulations relative to

529   PD are in ranges of 0.24–0.26, roughly 1.4 times the control run temperature

530   variability. This is in the expectation from subtracting two independent Gaussian

531   noise distributions. While there could be an additional contribution to variability from

532   BC-climate interactions, this appears to be small in this case given the relatively small

533   surface temperature response to BC. We also observe large variability in cloud

534   radiative effects, which we note may be impacted by interactions with BC.

535   While we have demonstrated non-linear responses at high emission levels, this

536   non-linearity is not sufficient to produce statistically significant global temperature

537   changes from present-day BC emissions in this model. Such non-linearities mean

538   that the implications of large BC emission perturbation experiments, such as recent

539   tenfold BC experiments (Stjern et al., 2017) for present-day conditions are unclear.

540   While snow/ice-albedo feedbacks appear to dominate the non-linear relationship in

541   these results, this may not be the case in other models.

542   Our results point to the importance of better quantifying the variability in BC

543   responses in the Earth system. We note that in the one model with a consistent PD-PI

544   signal in a set of recent PD-PI BC experiments (NorESM1-M), the size of that signal

545   is still smaller than the variability found here, based on similar SD in Arctic

546   temperature change for the ARC150X simulations in the two models (compare Figure

547   S3 here with Figure 9 in Sand et al. (2013b)). If the global variability of BC response

548   in NorESM is also similar to that in CESM, then the global average temperature

549   change from NorESM (0.141 K) (Baker et al., 2015) is also much smaller than the SD

550   in CESM of 0.238 K. However, we do note that there was a fair degree of consistency

551   in temperature change signal in NorESM between two ensemble members (0.129 K

552   and 0.152 K). This may mean that variability in the global BC response in the

553   NorESM model could be smaller than seen in our results due to the stronger NorESM

554   BC temperature response. Longer simulations would likely be required to assess this.

555   While, compared to temperature or precipitation, aerosol burdens, BC direct radiative

556   effects and snow/ice-albedo forcings have much larger signal to noise ratios, i.e. ratio

557   of mean response to standard deviation (Table 1), and can be useful as diagnostics,

558   BC forcing does not provide a reliable indicator of surface temperature changes

559   across models.

560   These results indicate that even substantial BC emissions reductions from

561   current levels may lead to detectable surface temperature changes for only limited

562   regions of the globe. Our results have significant implications for near-term climate

563   mitigation associated with BC as well as global and regional climate attribution. We

564   note that regional climate sensitivities (RCS), used as an approximate approach to

565   represent the impact of BC (Collins et al., 2013; Sand et al., 2016), are generally

566   evaluated using model simulations with prescribed forcing or burdens (Shindell and

567   Faluvegi, 2009), which artificially reduce response variability and imply a certainty in

568   BC responses that may not exist in reality. Variability within any given model run,

569   which has generally not been reported in current literature, is large relative to BC

570   responses. It is, therefore, not clear if current BC emission levels result in statistically

571   significant large-scale climatic changes. We suggest that impacts of BC on climate

572   should be expressed directly in terms of impacts per unit emissions (e.g. Table 1),

573   and not only relative to forcing given the complex relationship between BC climatic

574   impacts and top of the atmosphere forcing. In addition, BC impacts should be

575   re-evaluated using coupled models, and provided with measures of response

576   variability, such as standard deviation. In order to better assess the potential impact

577   of changes in BC emissions it is critical to quantify the non-linearity of BC response

578   efficiencies with respect to emission perturbation size in other models, as well as the

579   causes of those non-linearities.

580

581

582

583   ***Acknowledgments***.

591

592

References

Abdul-Razzak, H. and Ghan, S. J.: A parameterization of aerosol activation 2. Multiple aerosol types, J. Geophys. Res., 105, 6837–6844, doi:10.1029/1999JD901161, 2000.

Andrews, T., Forster, P. M., Boucher, O., Bellouin, N., and Jones, A.: Precipitation, radiative forcing and global temperature change, Geophys. Res. Lett., 37, L14701, doi:10.1029/2010GL043991, 2010.

Baker, L. H., Collins, W. J., Olivié, D. J. L., Cherian, R., Hodnebrog, Ø., Myhre, G., and Quaas, J.: Climate responses to anthropogenic emissions of short-lived climate pollutants, Atmos. Chem. Phys., 15, 8201-8216, doi:10.5194/acp-15-8201-2015, 2015.

Ban-Weiss, G. A., Cao, L., Bala, G., and Caldeira, K.: Dependence of climate forcing and response on the altitude of black carbon aerosols, Clim. Dyn., 38, 897–911, doi:10.1007/s00382-011-1052-y, 2012.

Betancourt, M.: A conceptual introduction to Hamiltonian Monte Carlo, arXiv preprint, arXiv:1701.02434, 2017.

Bond, T. C., Doherty, S. J., Fahey, D. W., Forster, P. M., Berntsen, T., DeAngelo,B. J., Flanner, M. G., Ghan, S., Kärcher, B., Koch, D., Kinne, S., Kondo, Y., Quinn, P. K., Sarofim, M. C., Schultz, M. G., Schulz, M., Venkataraman, C., Zhang, H., Zhang, S., Bellouin, N., Guttikunda, S. K., Hopke, P. K., Jacobson, M. Z., Kaiser, J. W., Klimont, Z., Lohmann, U., Schwarz, J. P., Shindell, D., Storelvmo, T., Warren, S. G., and Zender, C. S.: Bounding the role of black carbon in the climate system: A scientific assessment, J. Geophys. Res., 118, 5380–5552, doi:10.1002/jgrd.50171, 2013.

Boucher, O., Randall, D., Artaxo, P., Bretherton, C., Feingold, G., Forster, P., Kerminen, V.-M., Kondo, Y., Liao, H., Lohmann, U., Rasch, P., Satheesh, S. K., Sherwood, S., Stevens, B., and Zhang, X. Y.: Clouds and Aerosols, in: Climate Change 2013: The Physical Science Basis, Contribution of Working Group I to the Fifth Assessment Report of the Intergovernmental Panel on Climate Change, edited by: Stocker, T. F., Qin, D., Plattner, G.-K., Tignor, M., Allen, S. K., Boschung, J., Nauels, A., Xia, Y., Bex, V., and Midgley, P. M., Cambridge University Press, Cambridge, United Kingdom and New York, NY, USA, 571–658, doi:10.1017/CBO9781107415324.016, 2013.

Boucher, O. and Reddy, M. S.: Climate trade-off between black carbon and carbon dioxide emissions, Energ. Policy, 36, 193–200, doi:10.1016/j.enpol.2007.08.039, 2008.

637

638 Collins, W. J., Fry, M. M., Yu, H., Fuglestvedt, J. S., Shindell, D. T., and West, J. J.:
639 Global and regional temperature-change potentials for near-term climate forcers,
640 Atmos. Chem. Phys., 13, 2471-2485, https://doi.org/10.5194/acp-13-2471-2013,
641 2013.
642

643 Flanner, M. G.: Arctic climate sensitivity to local black carbon, J. Geophys. Res.
644 Atmos., 118, 1840–1851, doi:10.1002/jgrd.50176, 2013.
645

646 Flanner, M. G., Zender, C. S., Randerson, J. T., and Rasch, P. J.: Present day
647 climate forcing and response from black carbon in snow, J. Geophys. Res., 112,
648 D11202, doi:10.1029/2006JD008003, 2007.
649

650 Geoffroy, O., Saint-Martin, D., Bellon, G., Voldoire, A., Olivié, D. J., and Tytéca, S.:
651 Transient climate response in a two-layer energy-balance model. Part II:
652 Representation of the efficacy of deep-ocean heat uptake and validation for
653 CMIP5 AOGCMs, J. Climate, 26, 1859–1876, doi:10.1175/JCLI-D-12-00196.1,
654 2013.
655

656 Gettelman, A., Liu, X., Ghan, S. J., Morrison, H., Park, S., Conley, A. J., Klein, S. A.,
657 Boyle, J., Mitchell, D. L., and Li, J. L. F.: Global simulations of ice nucleation and
658 ice supersaturation with an improved cloud scheme in the Community
659 Atmosphere Model, J. Geophys. Res., 115, D18216, doi:10.1029/2009jd013797,
660 2010.
661

662 Ghan, S. J.: Technical Note: Estimating aerosol effects on cloud radiative forcing,
663 Atmos. Chem. Phys., 13, 9971–9974, doi:10.5194/acp-13-9971-2013, 2013.
664

665 Hansen, J., Sato, M., Ruedy, R., Nazarenko, L., Lacis, A., Schmidt, G. A., Russell, G.,
666 Aleinov, I., Bauer, M., Bauer, S., Bell, N., Cairns, B., Canuto, V., Chandler, M.,
667 Cheng, Y., Del Genio, A., Faluvegi, G., Fleming, E., Friend, A., Hall, T., Jackman,
668 C., Kel- ley, M., Kiang, N., Koch, D., Lean, J., Lerner, J., Lo, K., Menon, S., Miller,
669 R., Minnis, P., Novakov, T., Oinas, V., Perlwitz, Ja., Perlwitz, Ju., Rind, D.,
670 Romanou, A., Shindell, D., Stone, P., Sun, S., Tausnev, N., Thresher, D., Wielicki,
671 B., Wong, T., Yao, M., and Zhang, S.: Efficacy of climate forcings, J. Geophys.
672 Res., 110, D18104, doi:10.1029/2005JD005776, 2005.
673

674 Hoesly, R. M., Smith, S. J., Feng, L., Klimont, Z., Janssens-Maenhout, G., Pitkanen,
675 T., Seibert, J. J., Vu, L., Andres, R. J., Bolt, R. M., Bond, T. C., Dawidowski, L.,
676 Kholod, N., Kurokawa, J.-I., Li, M., Liu, L., Lu, Z., Moura, M. C. P., O'Rourke, P.
677 R., and Zhang, Q.: Historical (1750–2014) anthropogenic emissions of reactive
678 gases and aerosols from the Community Emissions Data System (CEDS),
679 Geosci. Model Dev., 11, 369–408, doi:10.5194/gmd-11-369-2018, 2018.
680

681 Hurrell, J. W., Holland, M. M., Gent, P. R., Ghan, S., Kay, J. E., Kushner, P. J.,
682   Lamarque, J. F., Large, W. G., Lawrence, D., Lindsay, K., Lipscomb, W. H., Long,
683   M. C., Mahowald, N., Marsh, D. R., Neale, R. B., Rasch, P., Vavrus, S.,
684   Vertenstein, M., Bader, D., Collins, W. D., Hack, J. J., Kiehl, J., and Marshall, S.:
685   The Community Earth System Model A Framework for Collaborative Research, B.
686   Am. Meteorol. Soc., 94, 1339–1360, doi:10.1175/BAMS-D-12-00121.1, 2013.
687
688 Hwang, Y.-T., Frierson, D. M. W., and Kang, S. M.: Anthropogenic sulfate aerosol
689   and the southward shift of tropical precipitation in the late 20th century, Geophys.
690   Res. Lett., 40, 2845–2850, doi:10.1002/grl.50502, 2013.
691
692 Jacobson, M. Z.: Climate response of fossil fuel and biofuel soot, accounting for
693   soot's feedback to snow and sea ice albedo and emissivity, J. Geophys. Res.,
694   109, D21201, doi:10.1029/2004JD004945, 2004.
695
696 Johnson, B. T., Shine, K. P., and Forster, P. M.: The semi-direct aerosol effect:
697   Impact of absorbing aerosols on marine stratocumulus, Q. J. Roy. Meteor. Soc.,
698   130, 1407–1422, doi:10.1256/qj.03.61, 2004.
699
700 Koch, D. and Del Genio, A. D.: Black carbon semi-direct effects on cloud cover:
701   review and synthesis, Atmos. Chem. Phys., 10, 7685-7696,
702   doi:10.5194/acp-10-7685-2010, 2010.
703
704 Koren, I., Kaufman, Y. J., Remer, L. A., and Martins, J. V.: Measurement of the effect
705   of Amazon smoke on inhibition of cloud formation, Science, 303, 1342–1345, doi:
706   10.1126/science.1089424, 2004.
707
708 Kvalevåg, M. M., Samset, B. H., and Myhre, G.: Hydrological sensitivity to
709   greenhouse gases and aerosols in a global climate model, Geophys. Res. Lett.,
710   40, 1432–1438, doi:10.1002/grl.50318, 2013.
711
712 Liu, X., Ma, P.-L., Wang, H., Tilmes, S., Singh, B., Easter, R. C., Ghan, S. J., and
713   Rasch, P. J.: Description and evaluation of a new four-mode version of the Modal
714   Aerosol Module (MAM4) within version 5.3 of the Community Atmosphere Model,
715   Geosci. Model Dev., 9, 505–522, doi:10.5194/gmd-9-505-2016, 2016.
716
717 McFarquhar, G. M., Ghan, S., Verlinde, J., Korolev, A., Strapp, J. W., Schmid, B.,
718   Tomlinson, J. M., Wolde, M., Brooks, S. D., Cziczo, D., Dubey, M. K., Fan, J.,
719   Flynn, C., Gultepe, I., Hubbe, J., Gilles, M. K., Laskin, A., Lawson, P., Leaitch, W.
720   R., Liu, P., Liu, X., Lubin, D., Mazzoleni, C., Macdonald, A.-M., Moffet, R. C.,
721   Morrison, H., Ovchinnikov, M., Shupe, M. D., Turner, D. D., Xie, S., Zelenyuk, A.,
722   Bae, K., Freer, M., and Glen, A.: Indirect and Semi-Direct Aerosol Campaign
723   (ISDAC): The Impact of Arctic Aerosols on Clouds, B. Am. Meteorol. Soc., 92,
724   183–201, doi:10.1175/2010BAMS2935.1, 2011.

McFarquhar, G. M. and Wang, H.: Effects of Aerosols on Trade Wind Cumuli over the Indian Ocean: Model Simulations, Q. J. R. Meteorol. Soc., 132, 821–843, doi:10.1256/qj.04.179, 2006.

Meinshausen, M., Smith, S. J., Calvin, K., Daniel, J. S., Kainuma, M. L. T., Lamarque, J.-F., Matsumoto, K., Montzka, S. A., Raper, S. C. B., Riahi, K., Thomson, A., Velders, G. J. M., and van Vuuren, D. P. P.: The RCP greenhouse gas concentrations and their extensions from 1765 to 2300, Climatic Change, 109, 213–241, doi:10.1007/s10584-011-0156-z, 2011.

Ming, Y., Ramaswamy, V., and Persad, G.: Two opposing effects of absorbing aerosols on global-mean precipitation, Geophys. Res. Lett., 37, L13701, doi:10.1029/2010GL042895, 2010.

Morrison, H. and Gettelman, A.: A new two-moment bulk stratiform cloud microphysics scheme in the Community Atmosphere Model, version 3 (CAM3), Part I: Description and numerical tests, J. Clim., 21, 3642–3659, doi:10.1175/2008JCLI2105.1, 2008.

Oshima, N., Koike, M., Zhang, Y., Kondo, Y., Moteki, N., Takegawa, N., and Miyazaki, Y.: Aging of black carbon in outflow from anthropogenic sources using a mixing state resolved model: Model development and evaluation, J. Geophys. Res., 114, D06210, doi: 10.1029/2008JD010680, 2009.

Qian, Y., Wang, H., Zhang, R., Flanner, M. G., and Rasch, P. J.: A sensitivity study on modeling black carbon in snow and its radiative forcing over the Arctic and Northern China, Environ. Res. Lett., 9, 064001, doi:10.1088/1748-9326/9/6/064001, 2014.

Ramanathan, V. and Carmichael, G.: Global and regional climate changes due to black carbon, Nat. Geosci., 1, 221–227, doi:10.1038/ngeo156, 2008.

Sand, M., Berntsen, T. K., Kay, J. E., Lamarque, J. F., Seland, Ø., and Kirkevåg, A.: The Arctic response to remote and local forcing of black carbon, Atmos. Chem. Phys., 13, 211-224, doi:10.5194/acp-13-211-2013, 2013a.

Sand, M., Berntsen, T. K., Seland, Ø., and Kristjánsson, J. E.: Arctic surface temperature change to emissions of black carbon within Arctic or midlatitudes, J. Geophys. Res. Atmos., 118, 7788–7798, doi:10.1002/jgrd.50613, 2013b.

Sand, M., Iversen, T., Bohlinger, P., Kirkevåg, A., Seierstad, I., Seland, Ø., and Sorteberg, A: A standardized global climate model study showing unique

768   properties for the climate response to black carbon aerosols, J. Climate., 28,
769   2512–2526, doi:10.1175/JCLI-D-14-00050.1, 2015.
770
771 Sand, M., Berntsen, T. K., von Salzen, K., Flanner, M. G., Langner, J., and Victor, D.
772   G.: Response of Arctic temperature to changes in emissions of short-lived climate
773   forcers, Nat. Clim. Change, 6, 286–289, doi:10.1038/nclimate2880, 2016.
774
775 Shindell, D.: Inhomogeneous forcing and transient climate sensitivity, Nat. Clim.
776   Change, 4, 274–277, doi:10.1038/nclimate2136, 2014.
777
778 Shindell, D. and Faluvegi, G.: Climate response to regional radiative forcing during
779   the twentieth century, Nat. Geosci., 2, 294–300, doi:10.1038/ngeo473, 2009.
780
781 Shindell, D., Kuylenstierna, J. C. I., Vignati, E., van Dingenen, R., Amann, M., Klimont,
782   Z., Anenberg, S. C., Muller, N., Janssens-Maenhout, G., Raes, F., Schwartz, J.,
783   Faluvegi, G., Pozzoli, L., Kupiainen, K., Höglund-Isaksson, L., Emberson, L.,
784   Streets, D., Ramanathan, V., Hicks, K., Oanh, N. T. K., Milly, G., Williams, M.,
785   Demkine, V., and Fowler, D.: Simultaneously Mitigating Near-Term Climate
786   Change and Improving Human Health and Food Security, Science, 335, 183–189,
787   doi:10.1126/science.1210026, 2012.
788
789 Smith, S. J. and Mizrahi, A.: Near-term climate mitigation by short-lived forcers, Proc.
790   Natl. Acad. Sci., 110, 14202–14206, doi:10.1073/pnas.1308470110, 2013.
791
792 Stjern, C. W., Samset, B. H., Myhre, G., Forster, P. M., Hodnebrog, Ø., Andrews, T.,
793   Boucher, O., Faluvegi, G., Iversen, T., Kasoar, M., Kharin, V., Kirkevåg, A.,
794   Lamarque, J.-F., Olivieì, D., Richardson, T., Shawki, D., Shindell, D., Smith, C.,
795   Takemura, T., and Voulgarakis, A.: Rapid adjustments cause weak surface
796   temperature response to increased black carbon concentrations, J. Geophys.
797   Res. Atmos., 122, 11462–11481, doi:10.1002/2017JD027326, 2017.
798
799 Stohl, A., Aamaas, B., Amann, M., Baker, L. H., Bellouin, N., Berntsen, T. K., Boucher,
800   O., Cherian, R., Collins, W., Daskalakis, N., Dusinska, M., Eckhardt, S.,
801   Fuglestvedt, J. S., Harju, M., Heyes, C., Hodnebrog, Ø., Hao, J., Im, U.,
802   Kanakidou, M., Klimont, Z., Kupiainen, K., Law, K. S., Lund, M. T., Maas, R.,
803   MacIntosh, C. R., Myhre, G., Myriokefalitakis, S., Olivié, D., Quaas, J.,
804   Quennehen, B., Raut, J.-C., Rumbold, S. T., Samset, B. H., Schulz, M., Seland,
805   Ø., Shine, K. P., Skeie, R. B., Wang, S., Yttri, K. E., and Zhu, T.: Evaluating the
806   climate and air quality impacts of short-lived pollutants, Atmos. Chem. Phys., 15,
807   10529–10566, doi:10.5194/acp-15-10529-2015, 2015.
808
809 Stohl, A., Klimont, Z., Eckhardt, S., Kupiainen, K., Shevchenko, V. P., Kopeikin, V. M.,
810   and Novigatsky, A. N.: Black carbon in the Arctic: the underestimated role of gas

811 flaring and residential combustion emissions, Atmos. Chem. Phys., 13, 8833–
812 8855, doi:10.5194/acp-13-8833-2013, 2013.
813
814 van Marle, M. J. E., Kloster, S., Magi, B. I., Marlon, J. R., Daniau, A.-L., Field, R. D.,
815 Arneth, A., Forrest, M., Hantson, S., Kehrwald, N. M., Knorr, W., Lasslop, G., Li,
816 F., Mangeon, S., Yue, C., Kaiser, J. W., and van der Werf, G. R.: Historic global
817 biomass burning emissions for CMIP6 (BB4CMIP) based on merging satellite
818 observations with proxies and fire models (1750–2015), Geosci. Model Dev., 10,
819 3329–3357, doi:10.5194/gmd-10-3329-2017, 2017.
820
821 Wang, H., Easter, R. C., Rasch, P. J., Wang, M., Liu, X., Ghan, S. J., Qian, Y., Yoon,
822 J.-H., Ma, P.-L., and Vinoj, V.: Sensitivity of remote aerosol distributions to
823 representation of cloud–aerosol interactions in a global climate model, Geosci.
824 Model Dev., 6, 765-782, doi:10.5194/gmd-6-765-2013, 2013.
825
826 Wang, M., Larson, V., Ghan, S., Ovchinnikov, M., Schanen, D., Xiao, H., Liu, X., Guo,
827 Z., and Rasch, P.: A multiscale modeling framework model (superparameterized
828 CAM5) with a higher-order turbulence closure: Model description and low-cloud
829 simulations, J. Adv. Model. Earth Syst., 7, 484–509, doi:10.1002/2014MS000375,
830 2015.
831
832 Yang, Y., Russell, L. M., Xu, L., Lou, S., Lamjiri, M. A., Somerville, R. C. J., Miller, A.
833 J., Cayan, D. R., DeFlorio, M. J., Ghan, S. J., Liu, Y., Singh, B., Wang, H., Yoon,
834 J.-H., and Rasch, P. J.: Impacts of ENSO events on cloud radiative effects in
835 preindustrial conditions: Changes in cloud fraction and their dependence on
836 interactive aerosol emissions and concentrations, J. Geophys. Res. Atmos., 121,
837 6321–6335, doi:10.1002/2015JD024503, 2016a.
838
839 Yang, Y., Russell, L. M., Lou, S., Lamjiri, M. A., Liu, Y., Singh, B., and Ghan, S. J.:
840 Changes in Sea Salt Emissions Enhance ENSO Variability, J. Climate, 29, 8575–
841 8588, doi:10.1175/JCLI-D-16-0237.1, 2016b.
842
843 Yang, Y., Wang, H., Smith, S. J., Ma, P.-L., and Rasch, P. J.: Source attribution of
844 black carbon and its direct radiative forcing in China, Atmos. Chem. Phys., 17,
845 4319-4336, doi:10.5194/acp-17-4319-2017, 2017.
846
847 Yang, Y., Wang, H., Smith, S. J., Zhang, R., Lou, S., Qian, Y., Ma, P.-L., Rasch, P. J.:
848 Recent intensification of winter haze in China linked to foreign emissions and
849 meteorology, Sci. Rep., 8, 2107, doi:10.1038/s41598-018-20437-7, 2018a.
850
851 Yang, Y., Wang, H., Smith, S. J., Zhang, R., Lou, S., Yu, H., Li, C., and Rasch, P. J.:
852 Source apportionments of aerosols and their direct radiative forcing and
853 long-term trends over continental United States, Earth's Future, 6, 793–808,
854 doi:10.1029/2018EF000859, 2018b.

855

856 Yang, Y., Wang, H., Smith, S. J., Easter, R. C., and Rasch, P. J.: Sulfate aerosol in
857   the Arctic: Source attribution and radiative forcing, J. Geophys. Res. Atmos., 123,
858   1899–1918, doi:10.1002/2017JD027298, 2018c.

859

860 Zhang, R., Wang, H., Hegg, D. A., Qian, Y., Doherty, S. J., Dang, C., Ma, P.-L.,
861   Rasch, P. J., and Fu, Q.: Quantifying sources of black carbon in western North
862   America using observationally based analysis and an emission tagging technique
863   in the Community Atmosphere Model, Atmos. Chem. Phys., 15, 12805-12822,
864   doi:10.5194/acp-15-12805-2015, 2015a.

865

866 Zhang, R., Wang, H., Qian, Y., Rasch, P. J., Easter, R. C., Ma, P.-L., Singh, B.,
867   Huang, J., and Fu, Q.: Quantifying sources, transport, deposition, and radiative
868   forcing of black carbon over the Himalayas and Tibetan Plateau, Atmos. Chem.
869   Phys., 15, 6205-6223, doi:10.5194/acp-15-6205-2015, 2015b.

870

884

		ΔColumn Burden (mg m^{-2})			Burden Eff. (mg m^{-2} (Tg yr^{-1})$^{-1}$)			ΔDRE (W m^{-2})		
		60–90°N	28–60°N	Global	60–90°N	28–60°N	Global	60–90°N	28–60°N	Global
ARC150X		5.37 (±0.30)	1.34 (±0.05)	0.63 (±0.03)	0.425 (±0.024)	0.106 (±0.004)	0.050 (±0.002)	3.94 (±0.39)	0.83 (±0.04)	0.45 (±0.03)
MID7X		2.19 (±0.09)	3.97 (±0.09)	1.26 (±0.03)	0.106 (±0.004)	0.191 (±0.004)	0.061 (±0.001)	2.90 (±0.19)	2.49 (±0.09)	1.00 (±0.04)
		DRE Eff. (W m^{-2} (Tg yr^{-1})$^{-1}$)			ΔCRE (W m^{-2})			CRE Eff. (W m^{-2} (Tg yr^{-1})$^{-1}$)		
		60–90°N	28–60°N	Global	60–90°N	28–60°N	Global	60–90°N	28–60°N	Global
ARC150X		0.39 (±0.03)	0.11 (±0.00)	0.05 (±0.00)	−3.83 (±0.98)	−0.46 (±0.84)	−0.22 (±0.54)	−0.30 (±0.08)	−0.04 (±0.07)	−0.02 (±0.04)
MID7X		0.17 (±0.01)	0.22 (±0.01)	0.08 (±0.00)	−2.30 (±0.96)	−3.16 (±0.90)	−1.26 (±0.51)	−0.11 (±0.05)	−0.15 (±0.04)	−0.06 (±0.02)
		ΔSnow/ice-albedo Forcing (W m^{-2})			Snow/ice-albedo Eff. (W m^{-2} (Tg yr^{-1})$^{-1}$)			ΔT (K)		
		60–90°N	28–60°N	Global	60–90°N	28–60°N	Global	60–90°N	28–60°N	Global
ARC150X		1.26 (±0.08)	0.12 (±0.02)	0.10 (±0.01)	0.099 (±0.006)	0.010 (±0.002)	0.008 (±0.001)	2.13 (±0.65)	0.78 (±0.22)	0.48 (±0.26)
MID7X		0.53 (±0.05)	0.18 (±0.03)	0.07 (±0.01)	0.026 (±0.002)	0.009 (±0.001)	0.003 (±0.000)	0.48 (±0.79)	0.45 (±0.27)	0.23 (±0.26)
		T Sensitivity (K (Tg yr^{-1})$^{-1}$)			ΔP (mm day^{-1})			P Sensitivity (µm day^{-1} (Tg yr^{-1})$^{-1}$)		
		60–90°N	28–60°N	Global	60–90°N	28–60°N	Global	60–90°N	28–60°N	Global
ARC150X		0.169 (±0.052)	0.062 (±0.018)	0.038 (±0.020)	−0.043 (±0.079)	−0.011 (±0.066)	0.010 (±0.023)	−3.38 (±6.29)	−0.86 (±5.26)	0.77 (±1.84)
MID7X		0.023 (±0.038)	0.022 (±0.013)	0.011 (±0.012)	0.048 (±0.096)	−0.159 (±0.069)	−0.032 (±0.022)	2.34 (±4.61)	−7.67 (±3.34)	−1.52 (±1.04)

885
886

Table 2. BC burden, DRE, CRE, and snow/ice-albedo forcing efficiencies, T
sensitivity and P sensitivity over the Arctic (60–90°N), mid-latitudes (28–60°N) and
the globe between perturbed (ARC75X/ARC150X/MID3.5X/MID7X/MID14X) and PD
simulations. 1-σ for 80-annual means is shown in the parentheses. Bold values
between two simulations (ARC75X/ARC150X, MID3.5X/MID7X, and MID7X/MID14X)
indicates statistically significant changes with 95% confidence from a two-tailed
Student's t test.

|		ARC75X	ARC150X			MID3P5X	MID7X	MID14X
		Burden Eff. (mg m^{-2} (Tg yr^{-1})$^{-1}$)						
60–90°N		**0.406 (±0.021)**	**0.425 (±0.024)**			**0.095 (±0.005)**	**0.106 (±0.004)**	**0.124 (±0.004)**
28–60°N		**0.097 (±0.004)**	**0.106 (±0.004)**			**0.175 (±0.005)**	**0.191 (±0.004)**	**0.219 (±0.005)**
Global		**0.047 (±0.002)**	**0.050 (±0.002)**			**0.055 (±0.001)**	**0.061 (±0.001)**	**0.070 (±0.002)**
		DRE Eff. (W m^{-2} (Tg yr^{-1})$^{-1}$)						
60–90°N		**0.346 (±0.036)**	**0.312 (±0.031)**			**0.146 (±0.014)**	**0.140 (±0.009)**	**0.137 (±0.006)**
28–60°N		**0.069 (±0.005)**	**0.066 (±0.003)**			**0.129 (±0.006)**	**0.120 (±0.004)**	**0.112 (±0.003)**
Global		**0.038 (±0.003)**	**0.035 (±0.003)**			**0.051 (±0.003)**	**0.048 (±0.002)**	**0.046 (±0.001)**
		CRE Eff. (W m^{-2} (Tg yr^{-1})$^{-1}$)						
60–90°N		**−0.533 (±0.232)**	**−0.303 (±0.078)**			−0.091 (±0.166)	**−0.111 (±0.046)**	**−0.015 (±0.029)**
28–60°N		0.010 (±0.222)	−0.037 (±0.067)			**0.070 (±0.203)**	**−0.152 (±0.043)**	**0.129 (±0.035)**
Global		**−0.028 (±0.071)**	**−0.017 (±0.043)**			0.013 (±0.058)	**−0.061 (±0.025)**	**0.035 (±0.010)**
		Snow/ice-albedo Eff. (W m^{-2} (Tg yr^{-1})$^{-1}$)						
60–90°N		**0.151 (±0.011)**	**0.099 (±0.006)**			**0.030 (±0.003)**	**0.026 (±0.002)**	**0.020 (±0.002)**
28–60°N		**0.013 (±0.003)**	**0.010 (±0.002)**			**0.011 (±0.002)**	**0.009 (±0.001)**	**0.007 (±0.001)**
Global		**0.012 (±0.001)**	**0.008 (±0.001)**			**0.004 (±0.001)**	**0.003 (±0.000)**	**0.003 (±0.000)**
		T Sensitivity (K (Tg yr^{-1})$^{-1}$)						
60–90°N		**0.239 (±0.116)**	**0.169 (±0.052)**			0.042 (±0.098)	**0.023 (±0.038)**	**0.008 (±0.015)**
28–60°N		0.067 (±0.032)	0.062 (±0.018)			0.020 (±0.025)	**0.022 (±0.013)**	**0.015 (±0.005)**
Global		**0.040 (±0.035)**	**0.038 (±0.020)**			0.008 (±0.033)	**0.011 (±0.012)**	**0.005 (±0.005)**
		P Sensitivity (µm day-1 (Tg yr^{-1})$^{-1}$)						
60–90°N		−2.88 (±13.39)	−3.38 (±6.29)			1.73 (±10.85)	2.34 (±4.61)	1.86 (±2.06)
28–60°N		−0.96 (±9.45)	−0.86 (±5.26)			−7.69 (±8.90)	**−7.67 (±3.34)**	**−8.53 (±1.61)**
Global		0.31 (±3.10)	0.77 (±1.84)			−1.99 (±2.81)	−1.52 (±1.04)	−2.15 (±0.49)

Figures for Paper

898

899

900
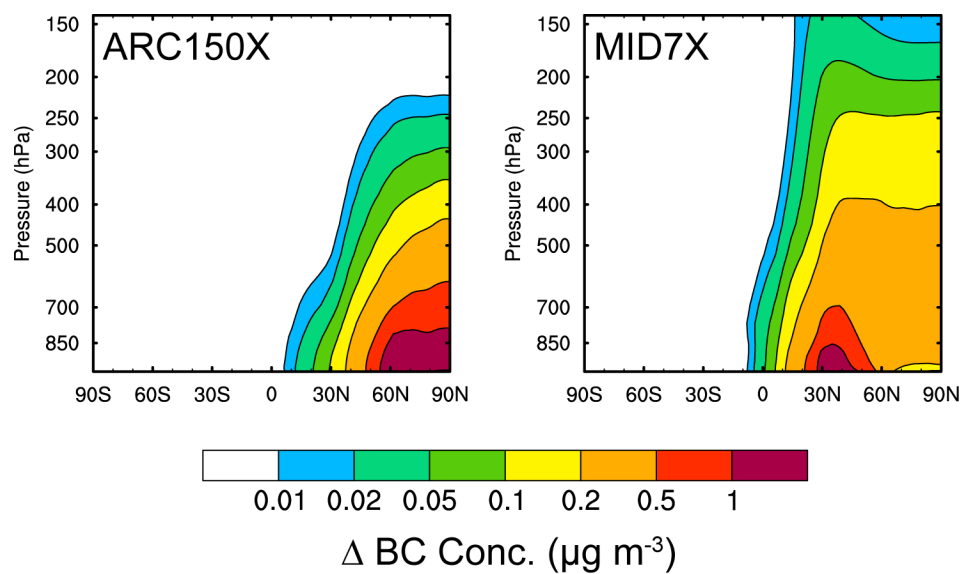
901   **Figure 1.** Difference in annual and zonal mean BC concentrations ($\mu g\ m^{-3}$) between

902   ARC150X (left)/MID7X (right) and PD simulations.
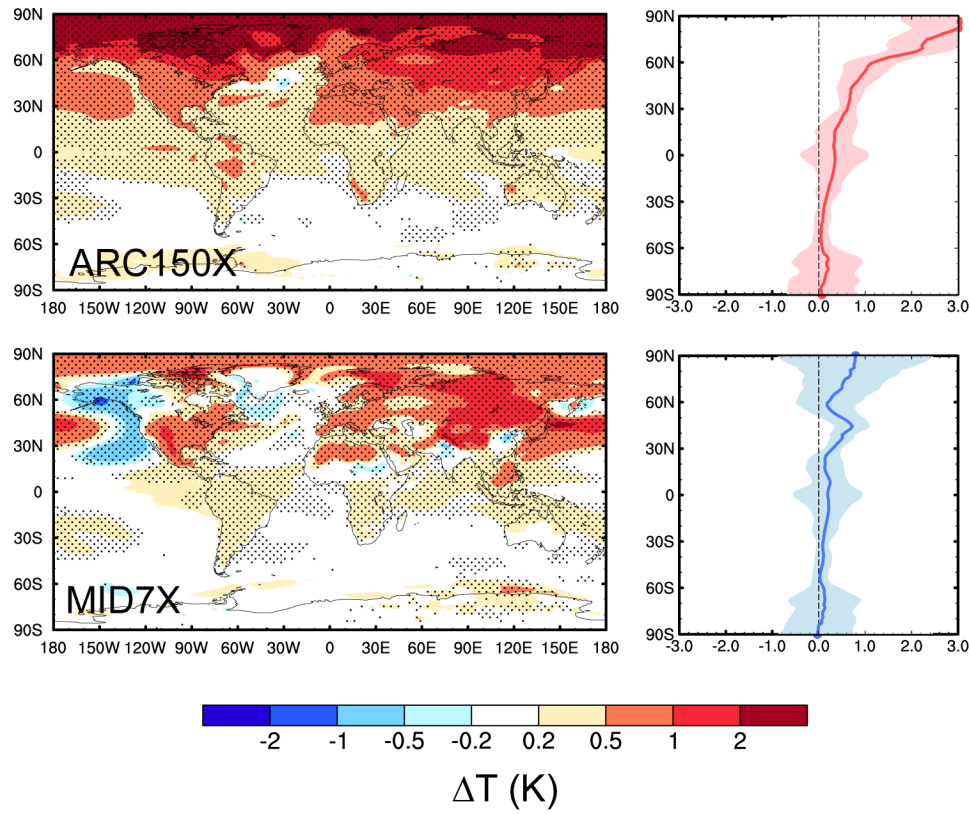
903

904

Figure 2. Spatial distribution (left) and zonal mean (right) of changes in annual mean surface air temperature (K) for ARC150X (top) and MID7X (bottom) compared to PD. The dotted areas in left panels indicate statistical significance with 95% confidence from a two-tailed Student's t test.
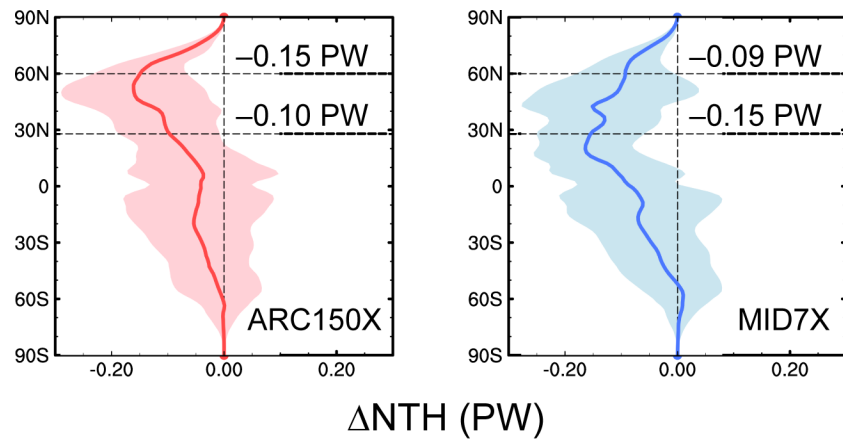
ΔNTH (PW)

Figure 3. Zonal mean of changes in annual mean northward heat transport (NHT, PW) for ARC150X (left) and MID7X (right) compared to PD. Values of changes in NHT across 60°N and 28°N are shown in each panel. The shaded areas represent 1-σ for 80-annual means.
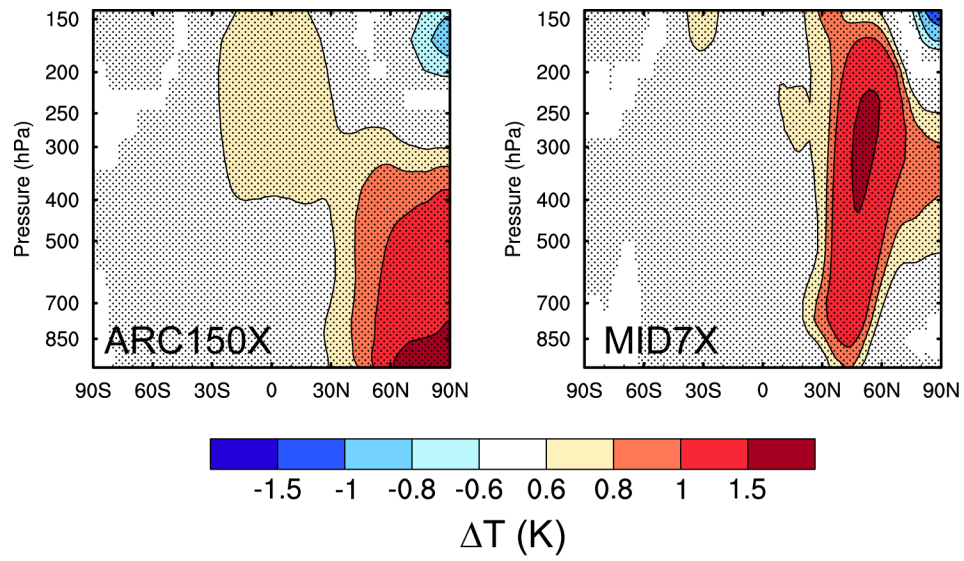
Figure 4. Changes in annual and zonal mean temperature (K) for ARC150X (left) and MID7X (right) compared to PD. The dotted areas indicate statistical significance with 95% confidence from a two-tailed Student's t test.
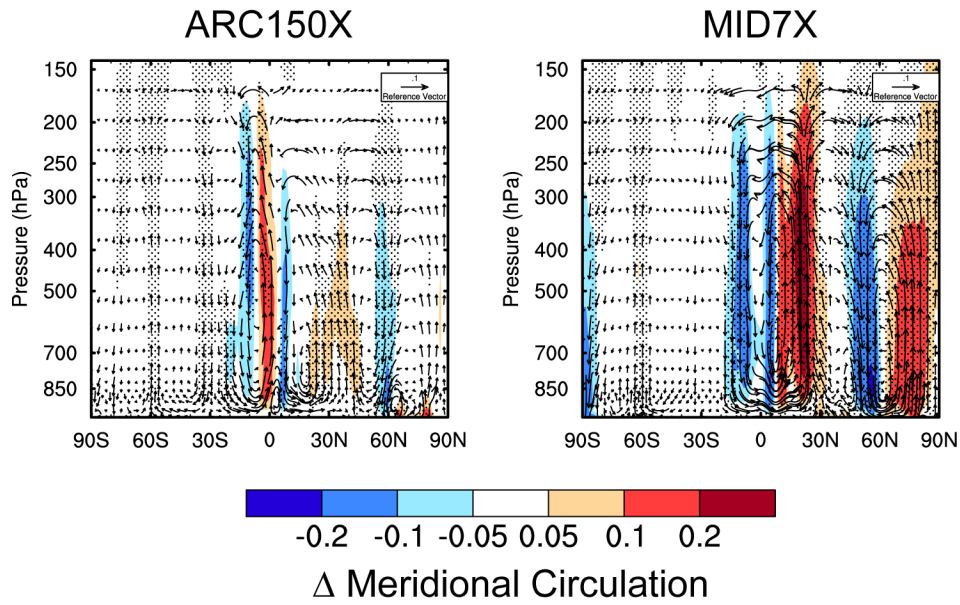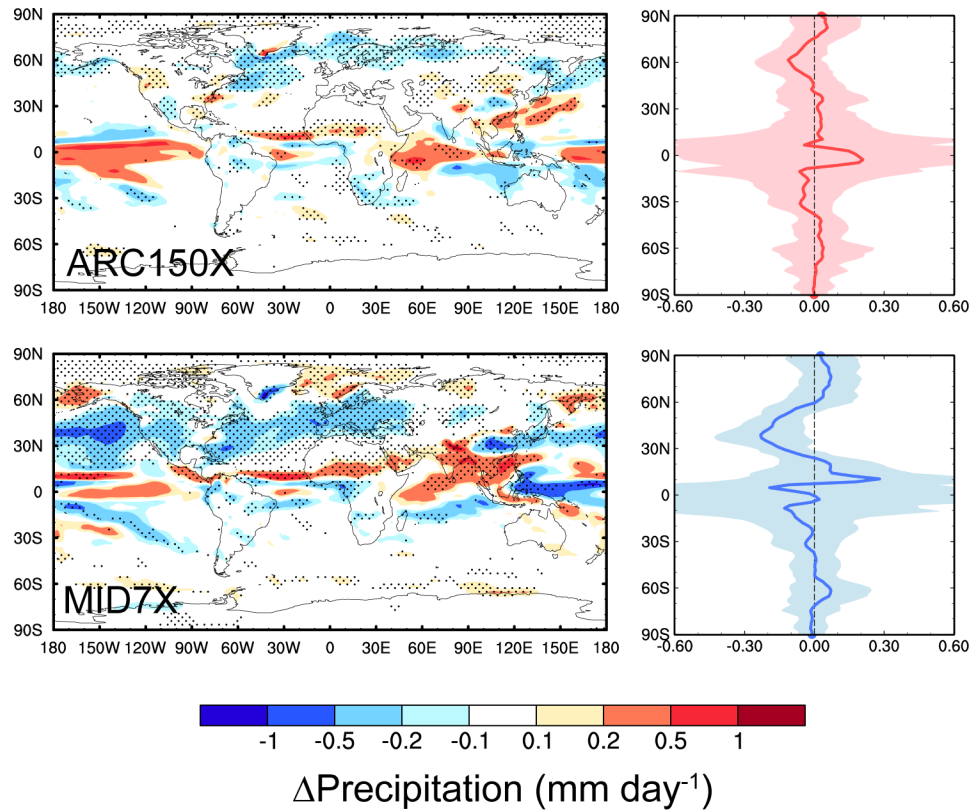
Figure 5. Changes in annual and zonal mean meridional wind vectors (m s^{-1}) and vertical velocity (contours; Pa s^{-1} scaled by a factor of -100) for ARC150X (left) and MID7X (right) compared to PD. The dotted areas indicate statistical significance with 95% confidence from a two-tailed Student's t test.
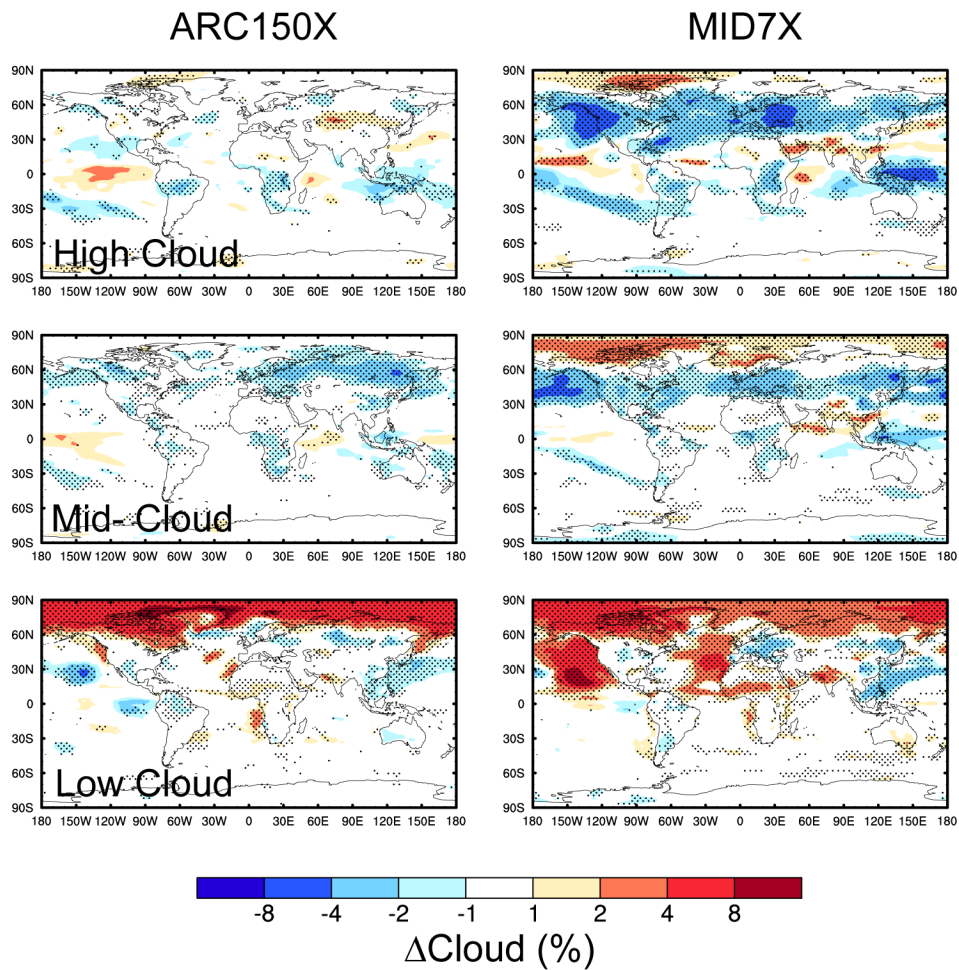
Figure 6. Changes in annual mean high (top), mid-level (middle), and low (bottom) cloud fraction (%) for ARC150X (left) and MID7X (right) compared to PD. The dotted areas indicate statistical significance with 95% confidence from a two-tailed Student's t test.

Figure 7. Spatial distribution (left) and zonal mean (right) of changes in annual mean total precipitation rate (mm day^{-1}) for ARC150X (top) and MID7X (bottom) compared to PD. The dotted areas in left panels indicate statistical significance with 95% confidence from a two-tailed Student's t test.
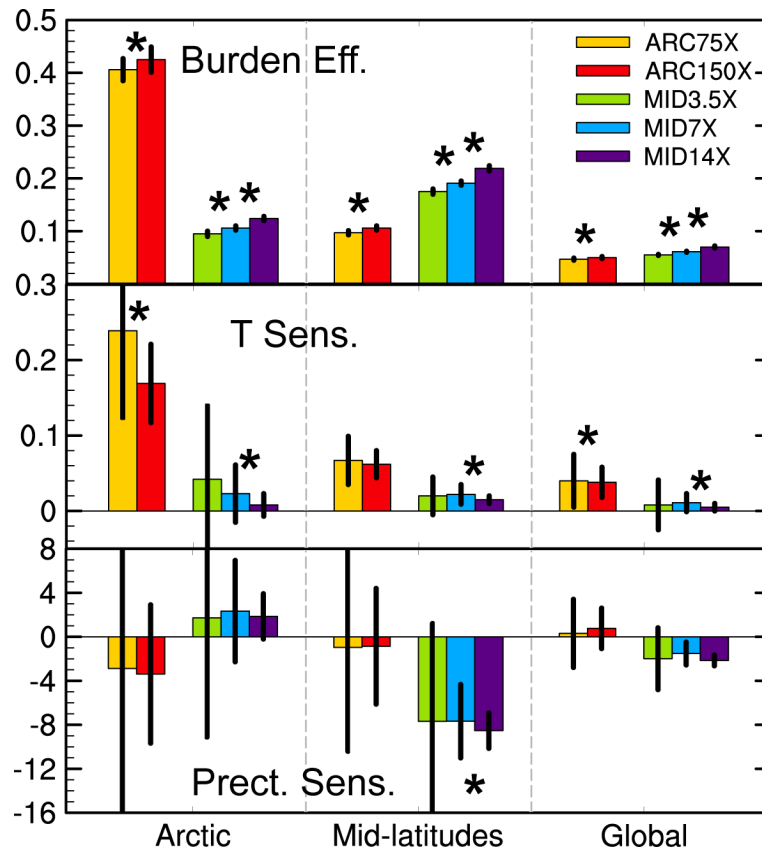
957

958

959 **Figure 8.** Burden efficiencies, temperature and precipitation sensitivities over the
960 Arctic, mid-latitudes and the whole globe for ARC75X, ARC150X, MID3.5X, MID7X
961 and MID14X. Burden efficiencies, temperature sensitivity and precipitation sensitivity
962 are calculated as changes in regional mean BC column burden, surface temperature
963 and total precipitation rate divided by changes in global total BC emissions between
964 perturbed and PD simulations, respectively. Error bars represent 1-σ for 80-annual
965 means. Asterisk between two bars (ARC75X/ARC150X, MID3.5X/MID7X, and
966 MID7X/MID14X) indicates statistically significant changes with 95% confidence from
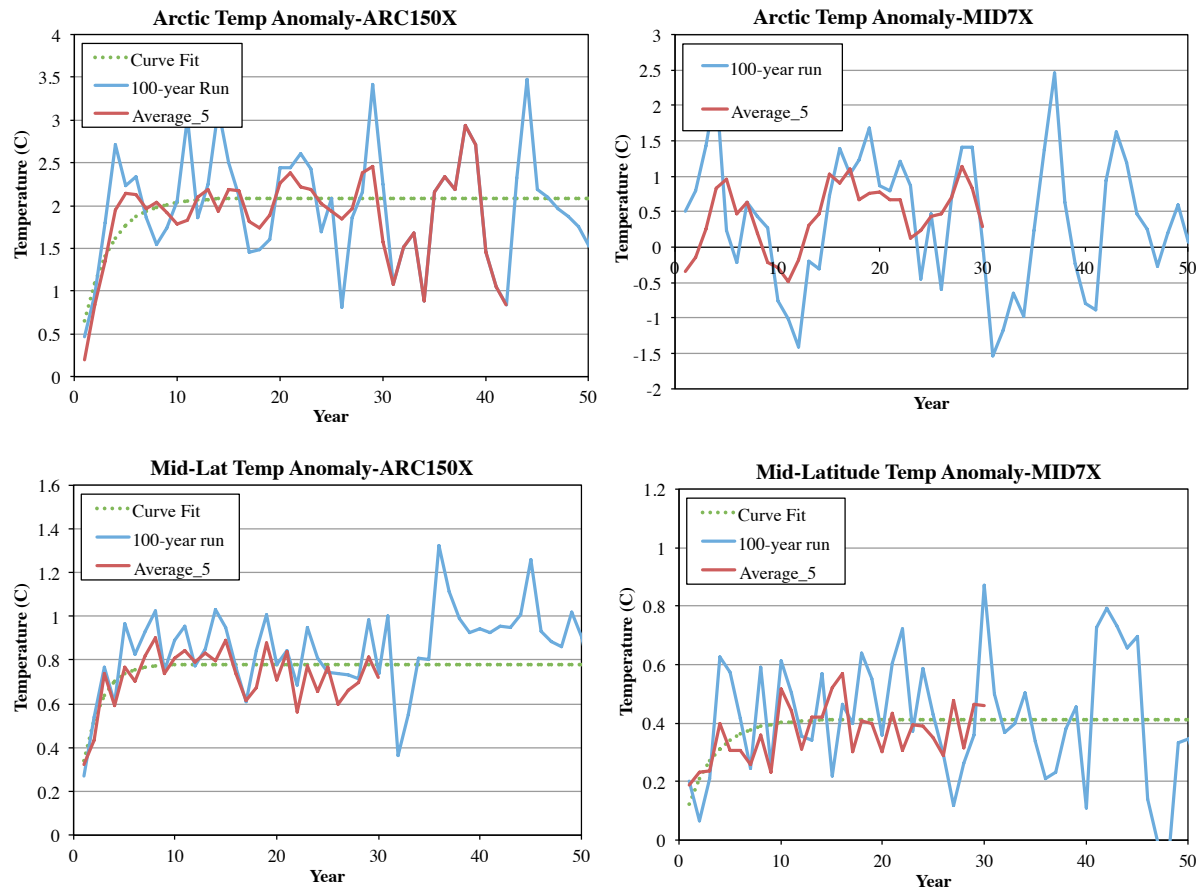967 a two-tailed Student's t test.

968

969

Figure 9. Time series of mean surface temperature response from ARC150X (left) and MID7X (right) BC emission perturbations as compared to PD. The response is shown over the Arctic (top) and mid-latitudes (bottom). Shown are the 100-year ensemble simulation (blue lines), the average of five 30-year ensemble members (red), and a numerical fit for an exponential approach to the long-term average (green dashed line). Curve fits used the package STAN in R, which is Bayesian inference using the No-U-Turn sampler. Note that MID7X Arctic temperature response does not result in a fit due to noise.
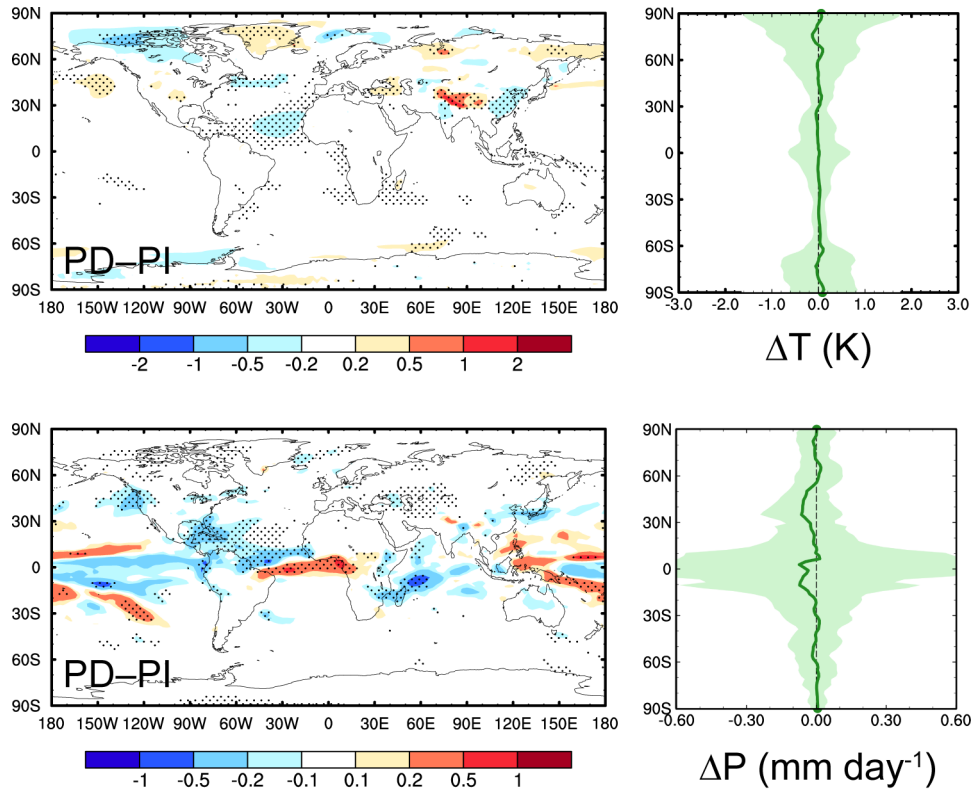
984
985
Figure 10. Spatial distribution (left) and zonal mean (right) of differences in annual
mean surface temperature (K, top) and total precipitation rate (mm day^{-1}, bottom)
between PD and PI. The dotted areas in left panels indicate statistical significance
with 95% confidence from a two-tailed Student's t test.

990
991